The Effect of Static Electrification on Gas−Solid Flows in Vertical Risers

ARTICLE *in* INDUSTRIAL & ENGINEERING CHEMISTRY RESEARCH · MARCH 2002

Impact Factor: 2.59 · DOI: 10.1021/ie010982w

3 AUTHORS, INCLUDING:

Sankaran Sundaresan
Princeton University
211 PUBLICATIONS **4,643** CITATIONS

SEE PROFILE

The Effect of Static Electrification on Gas−Solid Flows in Vertical Risers

Mahdi F. Al-Adel, Dudley A. Saville, and Sankaran Sundaresan*

Department of Chemical Engineering, Princeton University, Princeton, New Jersey 08544

Steady, fully developed gas−particle flow in a vertical riser is analyzed. The model consists of axial momentum balances for the gas and particle phases, a radial momentum balance for the particle phase, and Poisson's equation for the electric field. Each particle carries a prescribed charge. Consequently, a radially varying electric field develops spontaneously, and this drives an electrophoretic flux of particles toward the wall. This is balanced by a diffusive particle flux. At steady state, these fluxes balance and produce a radially nonuniform particle volume fraction distribution. This, in turn, affects the axial momentum balance. The model captures important qualitative features of riser flows: core−annular particle distribution, annular particle downflow at low riser gas velocities, and annular upflow at high gas velocities. Furthermore, the model accurately depicts results on riser flows reported by Bader et al.

1. Introduction

Although it has been known widely that static electrification can occur in gas−solid handling devices such as fluidized beds,[1−15] circulating fluidized beds,[16−23] and pneumatic conveying systems,[22−41] progress in understanding the influence of electrostatic charges on the mechanics has remained lethargic. Although considerable progress has been made in understanding charging mechanisms,[42−44] measuring or calculating electrical charges on particles in gas−particle systems is far from simple.[2] The charging is primarily a surface phenomenon, and the magnitude and sign of the charge are quite sensitive to the state of the surface and the characteristics of the ambient gas (e.g., humidity level and temperature).[3,5,6,11,18−21,31,34,37−39] Furthermore, in some systems, all of the particles appear to carry charges of the same sign (commonly referred to as *unipolar charging*); in others, some particles are positively charged, while others are negatively charged (*heteropolar charging*).[11,13,18] In the latter case, particles tend to agglomerate and complicate the hydrodynamics. In both cases, nonuniform particle distributions can arise on a macroscopic scale as a result of static electrification; this further impacts the hydrodynamics. For example, it is well-known that the pressure gradient required for the vertical conveying of particles by a gas depends on the extent of particle charging.[20,22,23,26,29,30,33,37,38] The excess pressure gradient, which can be attributed to the presence of charges on the particles, is often called the "electrostatic pressure gradient". There is ample evidence in the literature that increasing the humidity level (e.g., see ref 20) or adding antistatic agents[16] lowers the pressure gradient required for vertical conveying. In systems with unipolar charging, the electrostatic pressure gradient is intimately related to a nonuniform particle distribution over the pipe cross section.[41]

The nonuniform distribution of particles over the cross section is ubiquitous in gas−solids flows. In horizontal and inclined pneumatic transport lines, nonuniformities arise from gravitational sedimentation in the case of large particles. With finer particles, electrostatics plays a more important role.[32,41] Lateral segregation is also observed in vertical conveying (aka riser flows), and the origin of such segregation has been a subject of much research.[45−52] Gas−solid flows in risers are accompanied by density and velocity fluctuations that vary over a wide range of length and time scales, and these fluctuations cause lateral segregation.[45−52] In fact, all of the modeling efforts in this area have focused on hydrodynamic mechanisms for segregation. We are unaware of any modeling that includes static electrification as a significant driving force, even though the experimental evidence for the influence of electrostatics is striking.

In the present study, we examined the character and extent of lateral segregation arising from static electrification in riser flows. Hydrodynamically driven segregation was deliberately suppressed. A comprehensive model would predict the amount of charge carried by the particles and how it changes with flow conditions. Such a model is beyond the scope of the present study. Instead, we postulate that the particles carry a prescribed charge and then examine the influence of this charge on the hydrodynamics. The results of calculations made with our model are fully consistent with the fully developed flow patterns reported by Bader et al.[46] for FCC particles transported in a vertical riser. The level of unipolar particle charging required to capture the Bader et al.[46] data is comparable to that determined experimentally by Jiang et al.[18] Accordingly, our results demonstrate that electrostatic effects should be considered when analyzing gas−solid flows. At the very least, thorough, quantitative assessments should be made before their influence is ignored. It follows as a corollary that more experimental work probing static electrification in gas−solid flows is needed.

This paper is organized as follows. Section 2 presents a brief summary of literature data on electrostatic charges on particles in gas−solid flows. Here, we conclude that surface charge densities on the order of 10^{-7} C/m^2 (based on exterior surface area) are consistent with data reported by many researchers. Section 3

* To whom correspondence should be addressed. E-mail: sundar@princeton.edu. Phone: (609) 258-4583. Fax: (609) 258-0211.

10.1021/ie010982w CCC: $22.00
Published on Web 03/07/2002

Table 1. Summary of Data Reported by Ally and Klinzing[38]

tube material	particles	charge (μC/m^2)	kg of H_2O per kg of solid
copper	P004 glass, 75 μm	500	10^{-3}
	crushed glass, 314 μm	0.5	10^{-2}
	P008 glass, 150 μm	150	10^{-3}
	plexiglas, 145 μm	15	10^{-2}
plexiglas	P004 glass, 75 μm	50	10^{-3}
	P008 glass, 150 μm	15	10^{-3}
	plexiglas, 145 μm	120	10^{-2}
	copper, 196 μm	150	10^{-2}
glass	copper, 196 μm	2000	10^{-2}
	plexiglas, 145 μm	15000	10^{-3}

Table 2. Literature Data on Particle Charge in Pneumatic Conveying

material	charge density (μC/m^2)	reference
Illinois #2 coal (5 μm)	0.01	Gupta et al.[28]
charcoal (5 μm)	1.0	Gupta et al.[28]
latex (100 μm)	1−10	Nieh et al.[41]
alumina (60 μm)	1.0	Nieh et al.[41]
magnesia (30 μm)	0.01	Soo Trezek[40]
polystyrene (1 mm)	1−10	Gajewski[34]
plastic resin (30 μm)	4	Dahn[25]
plastic (20 μm)	0.6	Dahn[25]
flour (40 μm)	25.5	Dahn[25]
HDPE (3 mm)	0.9	Dahn[25]
glass beads (550 μm)	1−2	Nieh and Nguyen[39]
FCC particles (76 μm)	0.1−0.2	Jiang et al.[18]

describes a simple model for the steady, fully developed flow of a gas−particle mixture in a vertical pipe, where we assume that all of the particles are of the same size and carry the same amount of (unipolar) charge. In section 4, we describe our computational results and compare them with the data of Bader et al.[46] The key findings are summarized in section 5.

2. Literature Data on Static Electrification in Gas−Particle Flows

The electrostatic charge content of particles is usually reported in the literature on a mass basis (C/kg). We have converted all of these data to an (exterior) surface charge density using the reported particle size. Table 1 presents a summary of particle charge measured by Ally and Klinzing[38] in their experiments on pneumatic conveying in a 1-in. vertical pipe. It is clear from this table that the charge level depends on the tube material, particles, and humidity level.

Nieh and Nguyen[39] studied horizontal pneumatic transport of 550-μm glass beads in a 2-in. Cu pipe and found that the charge level increased with gas velocity and decreased with increasing humidity. A typical value for the surface charge density reported by these authors is 1 μC/m^2.

It is well-known that the variation of the pressure gradient with gas velocity (at a fixed particle flux) in vertical pneumatic conveying is U-shaped. Joseph and Klinzing[20] found that the location of the left limb was sensitive to the relative humidity (RH), which could be attributed to the dependence of the extent of static electrification on RH.

Table 2 summarizes data on charge accumulation on various materials during pneumatic conveying applications. Table 3 presents similar results obtained in the freeboard region of fluidized beds.

Chang and Louge[16] presented striking evidence for the effect of an antistatic agent on riser flow. At a specified combination of gas and plastic particle fluxes, the holdup of particles in the riser decreased appreciably (by over a factor of 2) upon the addition of an antistatic agent.

Table 3. Literature Data on Particle Charge in Fluidized Beds

material	charge density (μC/m^2)	reference
glass beads (35 μm)	1	Fasso et al.[15]
porcelain (2 μm)	0.1	Tardos and Pfeffer[14]
glass beads (200−250 μm)	0.1	Fujino et al.[2]
neobeads (200−540 μm)	0.1	Fujino et al.[2]
PMMA (540 μm)	0.1	Fujino et al.[2]
polyamide (75 μm)	0.003	Ali et al.[12]
polystyrene (475 μm)	1−10	Wolny and Kazmierczak[11]

Jiang et al.[18] studied the transport of FCC particles at a gas velocity of 2 m/s in a 10.2-cm-i.d. vertical pipe made of Plexiglas. They found that all of the particles carried the same sign of charge and that the charge level varied from 0.2 μC/m^2 at a RH of 14% to 0.1 μC/m^2 at a RH of 40%. The presence of the electrostatic charge was believed to have decreased the tendency of the particles to form clusters. (In systems such as polymer particles, the particles tend to acquire bipolar charges, and this enhances clustering.[18]) The charge level was found to be roughly independent of particle mass flux over the range studied [5−20 kg/(m^2 s)]. These authors found a measurable difference in the solids holdup profile with humidity level. For example, at a RH of 14% and a solids flux of 16.1 kg/(m^2 s), the volume fractions of particles in the core and wall regions were 0.01 and 0.04, respectively. At a RH of 40% and the same solids flux, the corresponding solids volume fractions were 0.018 and 0.032. Although the precise reason for the dependence of the particle concentration profile on humidity is not known, it is natural to suspect that static electrification might have been responsible. As RH increases, the charge level decreases, and the electrophoretic flux toward the wall is diminished.

It is clear from the data summarized here that the surface charge densities can vary widely from system to system. At the same time, one can also see that a surface charge density of ∼0.1 μC/m^2 is on the lower end of the range reported in the literature. It will become clear in section 4 that even such a small surface charge density can give rise to an appreciable radial segregation of particles in riser flows.

3. Model for Steady, Fully Developed Flow in a Riser

We use a simple model of steady, fully developed flow of gas−particle mixtures in a vertical pipe. It is assumed that the particles are uniform in size and that each carries the same amount of charge. Let the charge density (based on external surface area) be σ (C/m^2), so that each particle has a charge of $\pi d^2\sigma$. A radially varying electric field develops in the riser because of the charged particles. The structure of the field follows from the solution of Poisson's equation. This field imparts an electrical force on the particles, which causes them to drift toward the wall. This electrophoretic flux increases the concentration of particles near the wall region and decreases the concentration in the core. This flux is balanced by a diffusive flux of particles from the region of high ϕ (i.e., wall region) to the region of low ϕ

(i.e., tube axis). At steady state, these fluxes balance one another. The particles and the accompanying electrical effects influence the radial momentum balance in two ways. First, the electric field acting on the particles provides a body force. Second, the diffusive flux shows up as a gradient in the particle-phase pressure, $p_s(\phi)$.

The simple model presented here consists of steady-state axial momentum balances for the gas and particle phases, the Poisson equation for the electric potential and the steady-state radial momentum balance for the particle phase. To present these equations in dimensionless form we use the particle density (ρ_s), terminal velocity (v_t), tube radius (R), $\rho_s gR$ and $6R^2\sigma/\epsilon_o d$ as the characteristic density, velocity, length, pressure, and potential, respectively.

The axial momentum balance for the gas phase takes the form

$$-\frac{dp}{dz}+\frac{\phi}{(1-\phi)^{n-1}}(V_s-V_g)=0 \tag{1}$$

where p is the dimensionless pressure in the gas phase; z is the dimensionless axial variable (with the z axis pointing vertically upward); V_g and V_s are dimensionless gas- and solid-phase axial velocities, respectively; and n is the Richardson−Zaki exponent. The deviatoric stress term is not included as its role is negligible in flows with high solids mass loadings (e.g., see Agrawal et al.[52]).

The axial momentum balance for the particle phase takes the form

$$\frac{\phi}{(1-\phi)^{n-1}}(V_g-V_s)-\phi+\frac{1}{\xi}\frac{d}{d\xi}\left[\left(\frac{v_t\mu_s}{\rho_s gR^2}\right)\xi\frac{dV_s}{d\xi}\right]=0 \tag{2}$$

where the three terms represent the gas−particle drag, the body force due to gravity, and the viscous forces, respectively. Here, ξ and μ_s denote the dimensionless radial coordinate and dimensional viscosity associated with fluctuations at all length and time scales, respectively. The Archimedean buoyancy term is negligible in our work as $\rho_s\phi \gg \rho_g(1-\phi)$.

Poisson's equation, in dimensionless form, is

$$\frac{1}{\xi}\frac{d}{d\xi}\left[\epsilon(\phi)\xi\frac{d\Psi}{d\xi}\right]=-\phi \tag{3}$$

where Ψ is the dimensionless potential and $\epsilon(\phi)$ is the effective dielectric constant of the gas−solid mixture. Here, we have used a simple relation $\epsilon(\phi)=1+3.5\phi^{1.25}$ to represent the effect of the particles.The dielectric constant of the solid particles was taken to be 4.5, which is satisfied by this equation. This expression was obtained by curve-fitting the Bruggeman[61] equation for the effective dielectric constant of a mixture. We simply mention that we have repeated our simulations for various functional forms, including $\epsilon(\phi)=1+3.5\phi$ and $\epsilon(\phi)=1$, and verified that the general features of the solutions reported below are not dependent on the specific choice made for $\epsilon(\phi)$.

The radial momentum balance for the particle phase takes the form

$$\phi\left(\frac{36R\sigma^2}{\epsilon_o d^2\rho_s g}\right)\left(\frac{d\Psi}{d\xi}\right)+\left(\frac{1}{\rho_s gR}\right)\frac{dp_s}{d\xi}=0 \tag{4}$$

where the first term represents the force due to the electric field and the second term is the gradient in the particle-phase pressure. Here, the particle-phase pressure includes contributions arising from fluctuations at all velocity scales.

Closures for the particle-phase pressure and viscosity relations are needed before we can proceed further. Riser flows are accompanied by persistent fluctuations covering a wide range of length and time scales.[52] It is known that these fluctuations can give rise to a nonuniform distribution of particles over the cross section of a riser[45−52] even in the absence of any electrostatic effect. Sinclair and Jackson[45] attempted to explain this segregation of particles on the basis of fluctuations at the level of the individual particles. Dasgupta et al.[49] brought into the analysis the effect of velocity fluctuations occurring on a larger length scale through a $K-\epsilon$ model. Hrenya and Sinclair[51] proposed a model that combines the effects of the larger-scale and particle-scale fluctuations. Computational fluid dynamics simulations attempt to simulate the large-scale fluctuations occurring over a slow time scale and average over the fast fluctuations at short length and fast time scales (e.g., see Agrawal et al.[52]). Strictly speaking, if electrostatic effects are important, one should couple the hydrodynamic and electrostatic segregation mechanisms and analyze their combined influence. Here, however, we concentrate exclusively on segregation due to electrostatic effects and suppress all of the hydrodynamic segregation mechanisms. With this in mind, we choose a closure for the particle-phase pressure that curtails segregation in the absence of electrostatics. Accordingly, we employ the following expressions for the effective viscosity and pressure in the particle phase

$$\mu_s \equiv \mu_s^o\langle\phi\rangle = \rho_s\langle\phi\rangle\frac{UR}{300} \tag{5}$$

and

$$p_s=\frac{\rho_s\phi U^2}{400} \tag{6}$$

where U is the riser gas velocity, ϕ is the particle volume fraction (function of radial position), and $\langle\phi\rangle$ is the cross-sectional average particle volume fraction (i.e., holdup). Appendix A describes an analysis of fluctuations at different scales to support the choice of these relations.

Introducing these expressions into eqs 2 and 4, we have

$$\frac{\phi}{(1-\phi)^{n-1}}(V_g-V_s)-\phi+\frac{1}{\xi}\frac{d}{d\xi}\left(M_s^o\langle\phi\rangle\xi\frac{dV_s}{d\xi}\right)=0 \tag{7}$$

$$Q\phi\left(\frac{d\Psi}{d\xi}\right)+\frac{d\phi}{d\xi}=0 \tag{8}$$

where

$$M_s^o=\frac{\mu_s^o v_t}{\rho_s gR^2}=\frac{Uv_t}{300gR} \tag{9}$$

and

$$Q=\frac{(14400)R^2\sigma^2}{\epsilon_o d^2\rho_s U^2}. \tag{10}$$

These equations are supplemented with conditions at the axis of the tube, where center symmetry is enforced, and at the wall, where the electric potential assumes a specified value. As only a spatial derivative of the potential appears in the model, one can take

$$\Psi|_{\xi=1} = 0 \tag{11}$$

without loss of generality.

The particle-phase boundary condition at the wall is not fully understood. Some authors have suggested that the pressure gradient is almost completely associated with holdup in risers of large cross-sectional area;[16,62] thus, a free-slip condition for the particle phase is not unrealistic. Other possibilities, where one demands that the particle phase and/or the gas phase satisfies the no-slip condition (e.g., Gidaspow[50]), have also been discussed in the literature. A partial-slip boundary condition for the particle phase has also been applied (e.g., see Sinclair and Jackson[45]). We investigated both free-slip and no-slip boundary conditions for the particle phase to examine the sensitivity of the results to this boundary condition. The core−annulus flow pattern with downflow in the annular region at low gas velocities and annular upflow at high gas velocities is obtained with either boundary condition (Al-Adel[56]). To illustrate the role of electrostatics, we present results obtained with the free-slip boundary conditions here. With a free-slip boundary, one can readily show that

$$\frac{dp}{dz} = -\langle\phi\rangle$$

The cross-sectional average gas and solids fluxes can be written as

$$U_g^* = \frac{U_g}{v_t} = 2\int_0^1 \xi(1-\phi)V_g(\xi)\, d\xi \tag{12}$$

and

$$U_s^* = \frac{G_s}{\rho_s v_t} = 2\int_0^1 \xi\phi V_s(\xi)\, d\xi \tag{13}$$

where U_g and G_s denote the riser gas velocity and solids mass flux, respectively. The corresponding dimensionless quantities are U_g^* and U_s^*.

One can readily combine eqs 3 and 8, eliminate Ψ, and obtain an equation describing the radial variation of ϕ

$$\frac{1}{\xi}\frac{d}{d\xi}\left(\frac{\epsilon(\phi)}{Q\phi}\xi\frac{d\phi}{d\xi}\right) = -\phi$$

For specified values of Q and $\langle\phi\rangle$, this equation can be solved separately to determine the radial variation of ϕ. Thus, the radial distribution of particles is simply dictated by the charge density and the average holdup and is determined by the radial momentum balance and the Poisson equation. The average holdup for a *specified combination of fluxes* can be found only by solving the axial momentum balance equations.

We solved the complete system of equations 1, 3, 7, 8, 12, and 13 as a boundary-value problem by discretizing the spatial derivatives using a central difference scheme. For specified values of U_g^* and U_s^*, the solutions could be found for a range of values of Q by a simple continuation method. Specifically, starting from the analytical solution for $Q = 0$, the solutions for various Q values were found by changing Q by small increments (using the solution for the previous Q value as the initial guess). The average holdup, $\langle\phi\rangle$, is an output in such calculations. As discussed in the next section, turning points were encountered, with multiple solutions for some values of Q. A slightly different approach, where we specified $\langle\phi\rangle$, determined Q as an output, and performed continuation in $\langle\phi\rangle$, was computationally more expedient for tracing the family of solutions for a range of Q values.

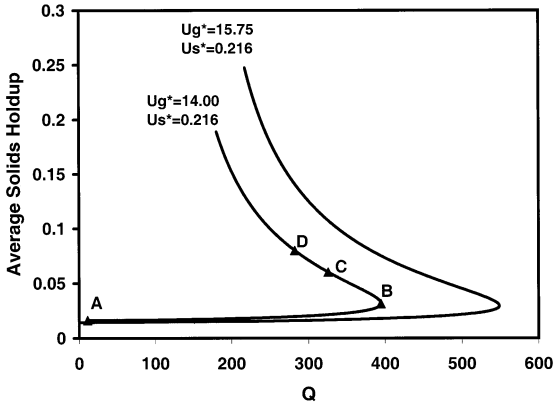

Figure 1. Average solids holdup vs Q for two different gas velocities at a fixed solid flux. See Table 4 for parameter values.

Table 4. Parameter Values Used in the Simulations

particle diameter	76 μm
particle density	1714 kg/m^3
terminal velocity	26.42 cm/s
riser radius	15 cm

Results and Discussion

Figure 1 shows the cross-sectional average holdup of particles in the riser, $\langle\phi\rangle$, as a function of Q for two combinations of U_g^* and U_s^*. The line labeled with four points (A−D) corresponds to conditions for which Bader et al.[46] reported experimental data. These authors studied the transport of FCC particles by ambient air in a 15-cm-i.d. vertical riser. Table 4 summarizes the parameter values corresponding to their experiments. They measured the radial variation of particle volume fraction (using γ-ray densitometry) at a gas velocity of 3.7 m/s and a solids mass flux of 98 kg/(m^2 s), which, in dimensionless form, corresponds to $U_g^* = 14.00$ and $U_s^* = 0.216$. (These authors also reported the radial variation of solids mass flux at another operating condition, which will be discussed later.) As noted in the Introduction, in the present study, we do not attempt to predict the value of σ for any operating conditions. Therefore, we cannot identify a specific value of Q for a specific experiment. It follows from eq 10 that $Q \approx O(10^3)$ when $\sigma \approx 10^{-7}$ C/m^2. Surface charge densities of this magnitude are easily achieved on FCC particles,[18] so the Q values explored in Figure 1 are quite reasonable.

Because we ignore hydrodynamic mechanisms for segregation in our model, the particle concentration is uniform when $Q = 0$. Hence, the velocity profile is uniform when a free-slip boundary condition is employed (and parabolic with a no-slip boundary condition). As Q increases, the average holdup increases (see Figure 1). This increase translates into an increase in

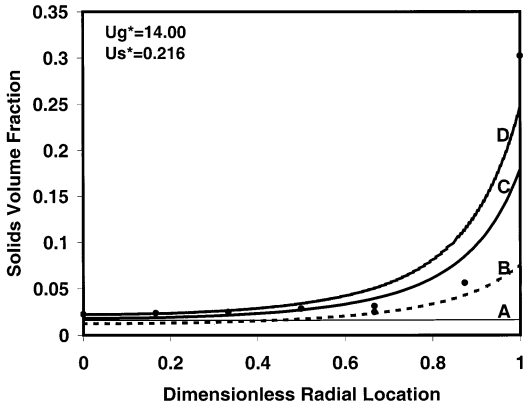

Figure 2. Particle volume fraction as a function of dimensionless radial position corresponding to the points A−D marked in Figure 1. (●) Experimental data of Bader et al.[46]

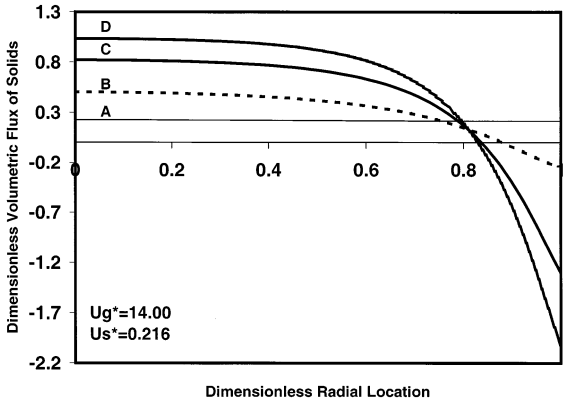

Figure 3. Dimensionless volumetric flux of solids as a function of dimensionless radial position corresponding to the points A−D marked in Figure 1.

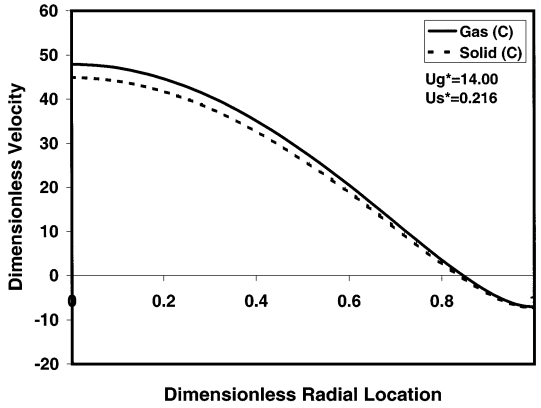

Figure 4. Dimensionless gas and solid velocities as a function of dimensionless radial position for point C in Figure 1.

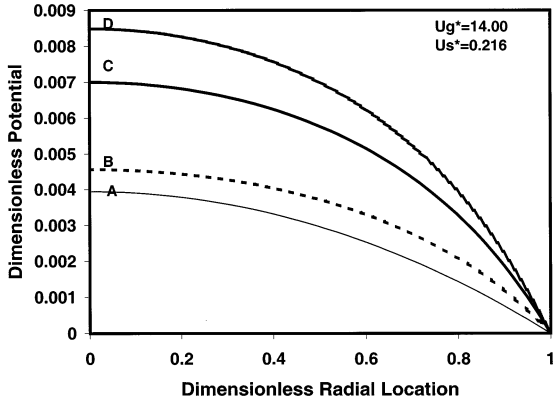

Figure 5. Dimensionless potential as a function of dimensionless radial position corresponding to the points A−D marked in Figure 1.

the pressure gradient, often called the *electrostatic pressure gradient* in pneumatic conveying.[20] Figure 1 shows that a turning point is encountered at a critical value of Q, so one can loosely talk of a lower branch and an upper branch.

The radial variations of the solids volume fraction for the four different points labeled A−D in one of the curves in Figure 1 are presented in Figure 2, along with the experimental data of Bader et al.[46] It is clear from Figure 2 that the extent of particle segregation increases steadily as the holdup increases (from A to D). Moreover, the core−annular flow structure is readily apparent at high segregation levels. The model predictions are qualitatively similar to the experimental data, although a quantitative match is not obtained for any particular value of Q. It should be noted, however, that, although the experimental data on radial variation of particle volume fraction obtained by γ-ray densitometry are qualitatively correct, they are by no means quantitatively accurate.

Figure 3 shows that radial variation of solids flux (ϕV_s) for the conditions shown in Figure 2; Figure 4 describes the gas- and particle-phase velocities for point C. It is clear from Figures 2 and 3 that, as the extent of radial segregation of particles increases, the solids flux becomes increasingly nonuniform. At sufficiently large segregation levels, one obtains downflow in the annular region with this example. Both particle and gas downflows are present as illustrated in Figure 4.

The radial profiles of the dimensionless potential for the cases shown in Figure 2 are displayed in Figure 5, which indicates that the largest magnitude of $d\Psi/d\xi$ occurs at the wall. In terms of dimensional quantities, the largest potential gradient was ~1 kV/cm (for case D in Figure 5), which is well below the field strength where dielectric breakdown occurs. Thus, the results shown in this figure are not unrealistic.

Figure 1 shows the holdup as a function of Q for two different gas velocities at a fixed solid flux. The general trend is clearly robust. As the gas velocity increases, the turning point shifts to larger Q values. Note that the upper branches of the curves in this figure have not been continued beyond some level. The only restriction placed in the mathematical model as presented is that $\phi < 1$. In reality, sustained contact between neighboring particles will occur when the particle volume fraction exceeds a threshold value, and the particle-phase pressure will rise rapidly with volume fraction beyond that point. Furthermore, it will be impossible to compress the assembly beyond some limit without crushing the particles, which is often taken in flow problems to be the volume fraction at random close packing, ϕ_{max}. Strictly speaking, the closures described in eqs 5 and 6 should be modified to capture this restriction; this point will be addressed briefly at the end of this paper. At this stage, we simply note that the curves in Figure 1 were terminated when the particle volume fraction at the wall is equal to ϕ_{max}.

Figure 6 shows the holdup as a function of Q for other operating conditions with the gas velocity held constant for changing solids flux. The shapes of the curves are qualitatively similar to those of Figure 1. The particle flux profile corresponding to four different points in one

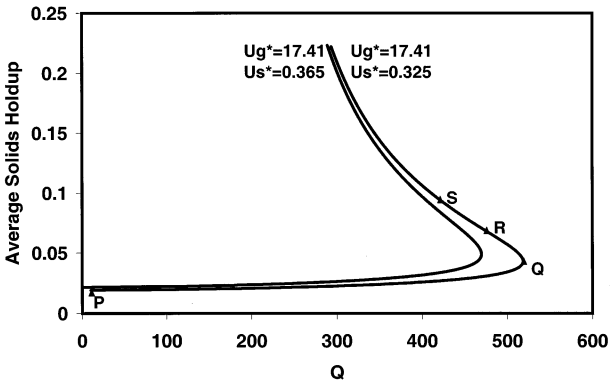

Figure 6. Average solids holdup vs *Q* for two different solid fluxes at a fixed gas velocity. See Table 4 for parameter values.

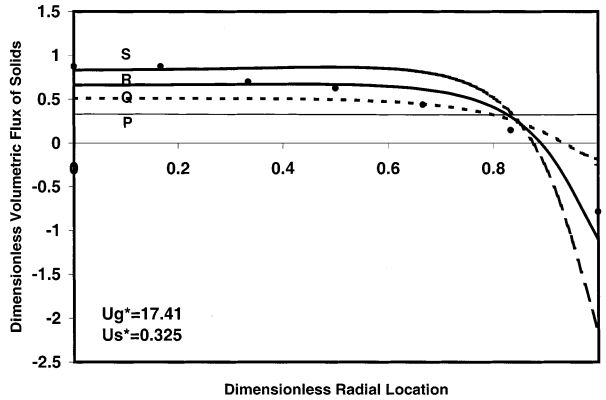

Figure 7. Dimensionless volumetric flux of solids as a function of dimensionless radial position corresponding to the points P−S marked in Figure 6. (●) Experimental data of Bader et al.[46]

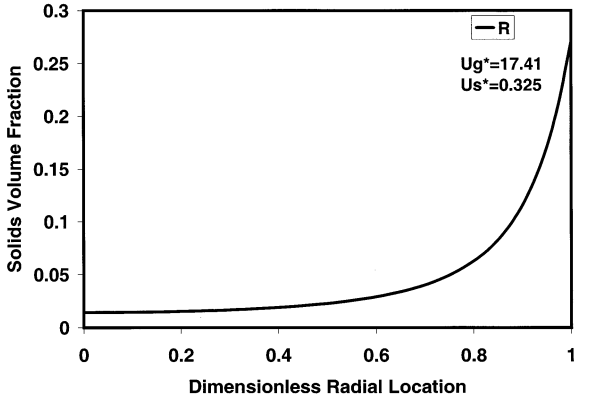

Figure 8. Particle volume fraction as a function of dimensionless radial position corresponding to point R in Figure 6.

of these curves is shown in Figure 7, with the experimental data of Bader et al.[46] The downflow in the annular region recorded by Bader et al. can be captured reasonably well by postulating the presence of an appropriate level of charge (e.g., that corresponding to point R). The solids volume fraction profile for point R in Figure 7 is displayed in Figure 8, where the core−annular flow structure is clearly apparent. The corresponding gas and solid velocity profiles are presented in Figure 9, which shows clearly the downflow of both the gas and the particles near the wall. The radial variation of the dimensionless potential for point R is illustrated in Figure 10; once again, the dimensional potential gradient is well below the dielectric breakdown field strength. Returning to Figure 6, one can see that, as the solids flux is increased at a fixed gas velocity,

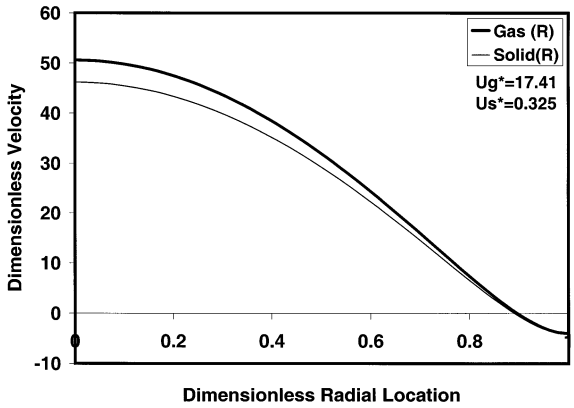

Figure 9. Dimensionless gas and solid velocities as a function of dimensionless radial position for point R in Figure 6.

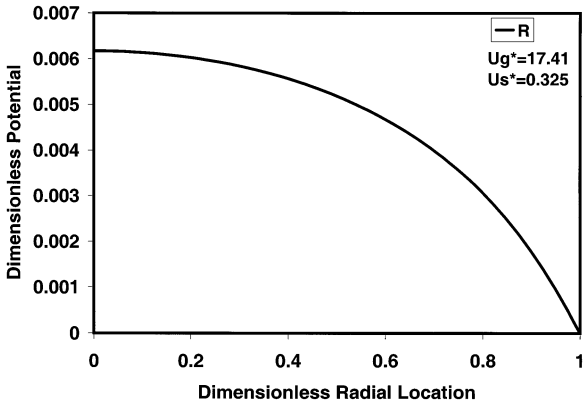

Figure 10. Dimensionless potential as a function of dimensionless radial position corresponding to point R in Figure 6.

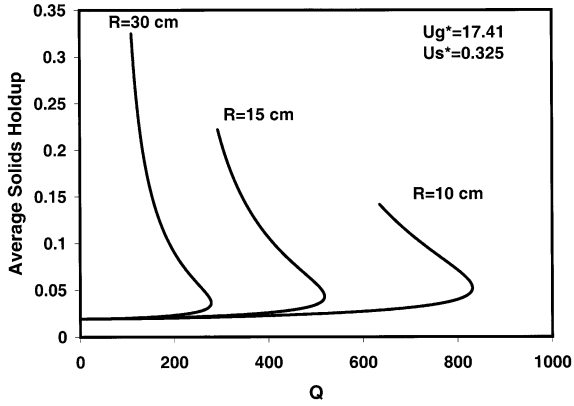

Figure 11. Average solids holdup vs *Q* for fixed gas and solid fluxes. Results are shown for three different tube radii. See Table 4 for parameter values.

the effect of electrostatics is felt at smaller and smaller values of *Q* (or, equivalently, at smaller surface charge densities).

Figure 11 shows the effect of the riser diameter for the same combinations of fluxes described in Figures 7−10. Note that the riser diameter has a systematic effect on the flow and that the effect of electrostatics becomes increasingly important as the tube diameter is increased.

Figure 12 shows the effect of increasing the throughput through the riser while maintaining the ratio of gas and solid fluxes constant. The curve labeled 1.0 corresponds to the combination of fluxes shown as the legend in this figure and has already been discussed in Figures

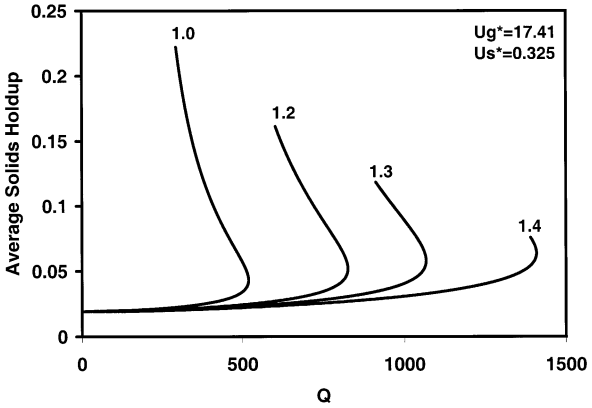

Figure 12. Average solids holdup vs Q for various gas and solid fluxes. The ratio of fluxes is held constant. The curve labelled 1.0 corresponds to the dimensionless gas and solid fluxes of 17.41 and 0.325, respectively. The dimensionless gas and solid fluxes for the other curves are simply obtained by multiplying 17.41 and 0.325 by the factors shown next to the curves. See Table 4 for other parameter values.

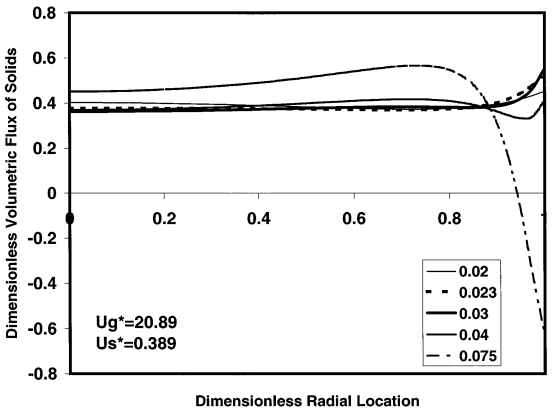

Figure 13. Dimensionless volumetric flux of solids as a function of dimensionless radial position for various points on the curve labeled 1.2 in Figure 12. The legends show the average solids holdups corresponding to the various curves.

7−10. The labels on the other curves simply refer to the multiple by which the fluxes (of both phases) have been increased from this base case. The turning point responds systematically to the throughput. The solids flux profiles corresponding to several different points on curves labeled 1.2 and 1.3 (in Figure 12) are shown in Figures 13 and 14, respectively. These figures reveal a flow feature that has received much attention in the literature recently, namely, annular upflow.[53−55] At modest levels of segregation (corresponding to intermediate holdup values in these figures), the peak flux occurs at the wall, and the peak location shifts inward as the holdup increases. These results should be contrasted with the flow patterns shown in Figures 3 and 7 for lower gas velocities, where the maximum upward flux occurs at the center.

We investigated briefly the effect of changing the closure for the particle-phase pressure given by eq 6. Specifically, we set

$$p_s = \frac{\rho_s \phi U^2}{400} g_o(\phi) \quad \text{where} \quad g_o(\phi) = \left(1 - \frac{\phi}{\phi_{max}}\right)^{-1/3} \tag{14}$$

which represents an ad hoc modification to ensure that the volume fraction of particles remains everywhere below ϕ_{max}. When this constraint is introduced into the

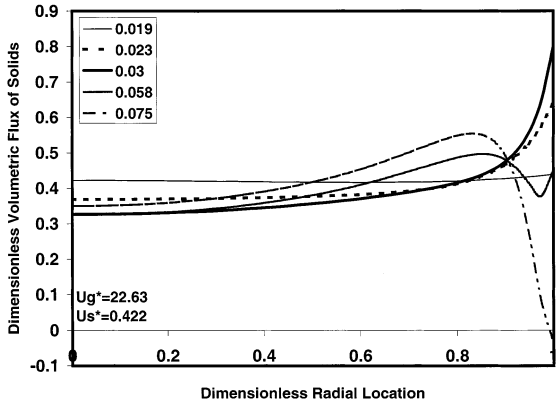

Figure 14. Dimensionless volumetric flux of solids as a function of dimensionless radial position for various points on the curve labeled 1.3 in Figure 12. The legends show the average solids holdups corresponding to the various curves.

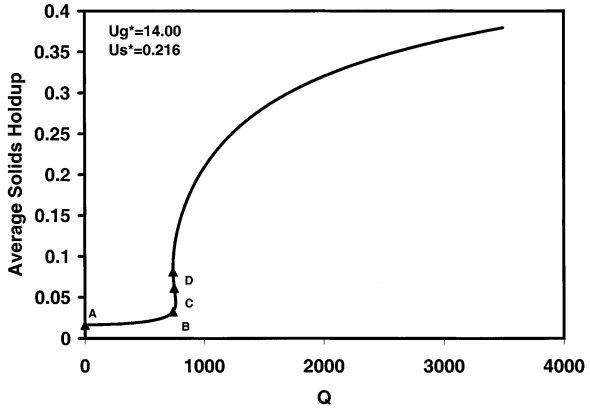

Figure 15. Average solids holdup vs Q for a specific combination of gas and solid fluxes. See Table 4 for parameter values. The particle-phase pressure is given by eq 14.

radial momentum balance, one obtains

$$Q\phi\left(\frac{d\Psi}{d\xi}\right) + \frac{d(\phi g_o)}{d\xi} = 0 \tag{15}$$

Figure 15 shows the variation of the holdup with Q obtained with this closure for the combination of fluxes discussed previously in Figures 1−5. Note that we now have an S-shaped curve in Figure 15, which should be contrasted with the corresponding curve in Figure 1. The points A−D marked in Figure 15 correspond to the same holdup values as in Figure 1 obtained with a simpler closure. The radial variations of the solids volume fraction and solids flux corresponding to these four points marked in Figure 15 are shown in Figures 16 and 17, respectively. These results should be compared with the curves shown in Figures 2 and 3. The addition of the g_o term has flattens the ϕ profile modestly, and its influence is felt in the solids flux profile. It is clear that, even though Figures 1 and 15 look significantly different, the general characteristics of the radial profiles remain robust. We simply note that the *annular upflow* obtained at high fluxes persists with the modified closure as well.

The present study clearly demonstrates that the lateral nonuniformities seen in riser flows can be captured in a qualitatively correct manner with a model that encompasses electrostatic effects. The amount of electrostatic charge required to fit the data is very modest and certainly lies in the lower range of values

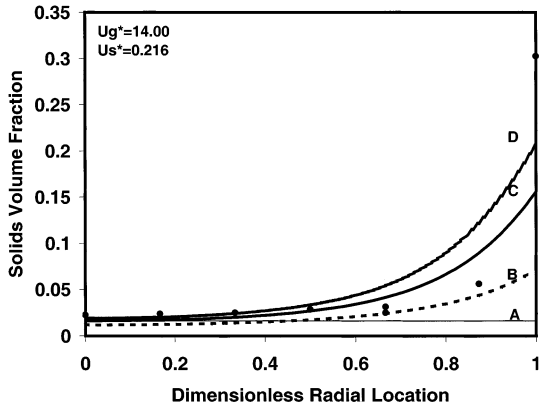

Figure 16. Particle volume fraction as a function of dimensionless radial position corresponding to the points A−D marked in Figure 15. (●) Experimental data of Bader et al.[46]

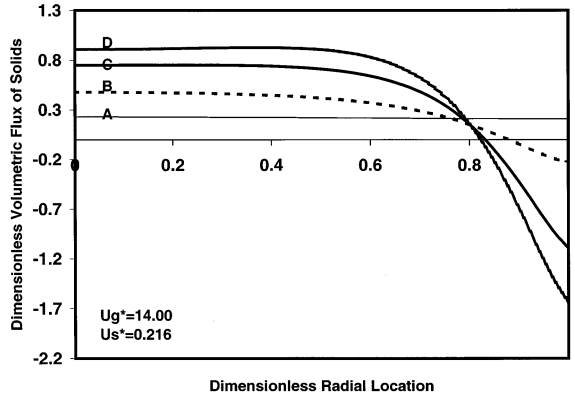

Figure 17. Dimensionless volumetric flux of solids as a function of dimensionless radial position corresponding to the points A−D marked in Figure 15.

reported in the literature. Thus, electrostatics should be considered carefully in future studies of gas−solid flows. In particular, careful experiments that probe the influence of static electrification on flow are needed.

In the present analysis, we suppressed hydrodynamically driven segregation. Thus, a natural extension will be to examine the combined influence of electrostatic and hydrodynamic segregation mechanisms. From the definition of Q, it follows that the effect of electrostatics decreases as particle size increases. Thus, we can anticipate that hydrodynamic segregation will be more relevant for larger particles, whereas electrostatic segregation will assume a greater importance with smaller particles.

A significant weakness of the present analysis derives from our ignorance about the size of the particle charges. At the same time, our study supports the need for more experimental and modeling work on the role of electrostatics in gas−solid flow. An obvious extension of the present model involves methods of describing the rates of generation and neutralization of particle charge, but closures for these processes remain a formidable challenge. In our opinion, experimental work to establish the relevance of electrostatics (or lack thereof) in gas−solid flows such as the riser flow analyzed here assumes a higher priority.

5. Summary

It is shown that electrostatics can be an important driving force for radial particle segregation in risers. Unfortunately, particle charge under a given set of conditions is unknown, and so, fully predictive models are not possible at this time. Consequently, a model of fully developed gas−particle flow was implemented with the charge level left as a model parameter. It was found that known trends, including core−annular flow, annular downflow at low gas velocities, and annular upflow at higher gas velocities, are captured with this model. In particular, experimental data for FCC particles by Bader et al.[46] can be captured by the model. The required charge level is at the lower end of the spectrum of charge levels reported in the literature.

Decades ago, Soo[35,40,41] and Owen[32] concluded that particle charge plays important roles in gas−particle flows with small particles. The results of the present study suggest that the lack of attention to this issue has been a grave oversight.

Appendix A

Simple Model for Particle-Phase Pressure and Viscosity. Consequences of Structures at Different Length Scales. It is well-known that hydrodynamic structures in the form of spatial and temporal nonuniformities in velocities and particle volume fractions are present in riser flows. These fluctuations span a wide range of length and time scales, and the origin of these structures is fairly well understood (e.g., Agrawal et al.[52]). It is also known that the segregation of particles toward the walls of the riser can occur simply because of hydrodynamic effects.[45−52] In this paper, we specifically suppress *hydrodynamically driven segregation* and focus on assessing segregation from electrostatic effects. The role of hydrodynamic fluctuations should not be completely ignored, as they impart the particle phase with an effective viscosity and a pressure. The analysis described below outlines the rationale behind the expressions for particle-phase viscosity and pressure used in the present study.

At the smallest scale, the particles execute a fluctuating motion over and above the mean velocity; this is quantified through the granular temperature.[46,47,50−52,57] The fluctuating motion comes about because of (a) velocity gradients in the riser and (b) relative motion between the particles and the suspending gas (e.g., see Koch and Sangani[58]). An estimate of the fluctuating velocity due to the shear is $2Ud/R$, where U is the average velocity of the gas through the pipe, R is the tube radius, and d is the particle diameter. For typical riser flows with FCC particles (say, $U = 7$ m/s, $d = 75$ μm, and $R = 15$ cm), $2Ud/R = 0.7$ cm/s. Velocity fluctuations arising from the relative motion between the gas and the particles scale with the mean slip velocity,[59] and for dilute systems, this is typically one-tenth of the terminal velocity, v_t.[52] The terminal velocity for the FCC particles considered here is about 25 cm/s. Thus, we anticipate that the "slip motion" is the primary source of fluctuations at the particle scale. The Stokes number for the FCC particles suspended by air is ∼O(10^2), and so, we expect that the damping of the fluctuating motion is primarily due to inelastic collisions.[52] The length scale relevant for the estimation of the viscosity is thus the mean free path between collisions. For low particle concentrations, one then finds that

$$\mu_s \approx (\rho_s \phi)(0.1 v_t)\left(\frac{d}{\phi}\right) = 0.1 \rho_s v_t d$$

$$p_s \approx (\rho_s\phi)(0.1v_t)^2 = 0.01\rho_s{v_t}^2$$

It is well-known that a uniform suspension of particles fluidized by a gas is unstable and that nonuniform mesoscale structures form readily.[52] The effective pressure and viscosity due to the mesoscale structures were estimated by Agrawal et al.[52] through computational experiments. Their simulations suggest the following typical values of the effective viscosity and pressure

$$\mu_s \approx 0.5\rho_s{v_t}^3\frac{\phi}{g}, \quad p_s \approx 0.5\rho_s\phi{v_t}^2$$

which are significantly larger than the microscale viscosity and pressure.

Finally, there are fluctuations at the scale of the riser radius itself. Here, we expect that the scale of the fluctuations will manifest some dependence on the mean flow rate and the riser diameter. Unfortunately, there is no simple way of estimating the consequence of fluctuations at this scale. Detailed models based on particle-phase turbulence have been described in the literature where the hydrodynamic mechanism for segregation is also considered. As mentioned before, we want to consider only a very simple model for the effect of riser scale fluctuations here. Specifically, we wish to set aside the segregation that arises because of hydrodynamics and focus only on the possible segregation due to electrostatics alone. With this in mind, we ignore the lateral variation of the kinetic energy per unit mass associated with these fluctuations.[49,51] Instead, we simply take the fluctuating velocity and the mixing length to be a fraction of the mean gas velocity and the tube radius, respectively.

It is known from tracer gas dispersion measurements[60] that $UR/D_r \approx 300$, where D_r is the average value of the radial dispersion coefficient in the *core region* (where the particle concentration is roughly uniform). One can rationalize this physically as

$$D_r = v'l, \quad v' \approx \frac{U}{20}, \quad l \approx \frac{R}{15}$$

where $\approx$ indicates physically reasonable, typical values. As dispersion is associated with hydrodynamic fluctuations and fluctuations in the gas and particle phases are closely coupled,[52] the particle-phase dispersion coefficient can be expected to be comparable to that for the gas. Furthermore, we expect the effective kinematic viscosity, ν_s, to be roughly equal to the particle-phase dispersion coefficient as well. Thus, $\nu_s \approx v'l$. This suggests an expression for the particle-phase viscosity of the form $\mu_s \approx (\rho_s\phi)v'l$.

From the lessons of single-phase turbulent flow, one can anticipate that the mixing length will decrease as one approaches the wall. In the present two-phase flow problem, the particle concentration increases as one approaches the wall. For the sake of simplicity, we hypothesize that the radial variations of ϕ and l compensate each other and postulate that the particle-phase viscosity is roughly constant, independent of the radial position, and write

$$\mu_s = \rho_s\langle\phi\rangle\frac{UR}{300}$$

where $\langle\phi\rangle$ denotes the cross-sectional average volume fraction (holdup) of particles.

For the transport of FCC particles in a 30-cm-diameter riser at a gas velocity of 5 m/s, the ratio of the intermediate-scale viscosity to the macroscale viscosity is

$$\frac{150{v_t}^3}{URg} = 0.375$$

so that the macroscale viscosity is indeed the most relevant one. At higher gas velocities and tube diameters, the macroscale viscosity becomes even more dominant.

With this in mind, we use the following expression for viscosity in our model

$$\mu_s = \rho_s\langle\phi\rangle\frac{UR}{300} \tag{A1}$$

To be consistent, for the particle-phase pressure, we should use

$$p_s \approx \rho_s\phi(v')^2 = \frac{\rho_s\phi U^2}{400} \tag{A2}$$

It should be emphasized that these functional forms were chosen to ensure that the particle volume fraction will be uniform over the cross section of the riser in the absence of electrostatic effects, i.e., hydrodynamic segregation is not permitted.

It is interesting to compare the pressure obtained from the riser-scale fluctuations with that at the mesoscale. Typically, for riser flows, $U \approx 3-10$ m/s, so that $(U/20) \approx 15-50$ cm/s. At the lower end, this is not much different from the terminal velocity. Thus, the magnitude of the effective pressure due to the macroscale fluctuations is 1−10 times that due to fluctuations at the mesoscale.

The expressions for particle-phase viscosity and pressure described above, eqs A1 and A2, do not include the finite-size effect and thus allow the particle volume fraction at some regions of the riser to exceed the close-packing limit. This can be prevented by forcing the pressure and/or viscosity to become very large (diverge) at some critical volume fraction, ϕ_{max}. The qualitative arguments considered here do not shed any light on how this should be done. In some of the later examples described in this study, we demonstrated how the results will change if we replace eq A2 with

$$p_s = \frac{\rho_s\phi U^2}{400}g_o(\phi) \quad \text{where} \quad g_o(\phi) = \left(1 - \frac{\phi}{\phi_{max}}\right)^{-1/3} \tag{A3}$$

Acknowledgment

This work was supported by the New Jersey Commission on Science and Technology; Merck & Co., Inc.; and the ExxonMobil Research & Engineering Company. Financial support for M.F.A. by Saudi Aramco is gratefully acknowledged.

Nomenclature

d = particle diameter
D_r = radial dispersion coefficient of gas in the core region
g = acceleration due to gravity
g_o = function defined by eq A3
G_s = solids mass flux through the riser

L = characteristic length associated with fluidization instability
M_s^o = dimensionless solid-phase viscosity
n = Richardson−Zaki exponent (4.65)
p = dimensionless gas pressure
p_s = particle-phase pressure
Q = electrodiffusion parameter
R = riser radius
U = riser gas velocity
U_g^*, U_s^*= dimensionless riser gas and solids velocities, respectively
V_g, V_s = dimensionless gas and solid-phase axial velocities, , respectively, where the terminal velocity of the particle is used to make the velocities dimensionless
v_t = terminal velocity of the particle
v' = magnitude of the fluctuating velocity
l = mixing length
β = drag coefficient
ρ_s = particle density
μ_s = particle-phase viscosity
ν_s = particle-phase kinematic viscosity
ϵ = dielectric constant of the gas−solid mixture, a function of ϕ
ϵ_o = permittivity of free space [8.8542×10^{-12} C^2/(N m^2)]
ϕ = particle volume fraction (function of radial position)
$\langle\phi\rangle$ = cross-sectional average particle volume fraction (i.e., holdup)
Ψ = dimensionless electric potential (function of position)
ξ = dimensionless radial coordinate
σ = surface charge density (C/m^2)

Literature Cited

(1) Boland, D.; Al-Salim, Q. A. W.; Geldart, D. Static electrification in fluidized beds. *Chem. Eng. Sci.* **1969**, *24*, 1389−1390.

(2) Fujino, M.; Ogata, S.; Shinohara, H. The electric potential distribution profile in a naturally charged fluidized bed and its effects. *Int. Chem. Eng.* **1985**, *25*, 149−159.

(3) Ciborowski, J.; Woldarski, A. On electrostatic effects in fluidized beds. *Chem. Eng. Sci.* **1962**, *17* (1), 23−32.

(4) Briens, C. L.; Bergougnou, M. A.; Inculet, I. I.; Baron, T.; Hazlett, J. D. Size distribution of particles entrained from fluidized beds: Electrostatic effects. *Powder Technol.* **1992**, *70*, 57−62.

(5) Bafrnec, M.; Bena, J. Quantitative data on the lowering of electrostatic charge in a fluidized bed. *Chem. Eng. Sci.* **1972**, *27*, 1177−1181.

(6) Guardiola, J.; Rojo, V.; Ramos, G. Influence of particle size, fluidization velocity and relative humidity on fluidized bed electrostatics. *J. Electrost.* **1996**, *37*, 1−20.

(7) Park, A.-H. A. Electrostatic charging in gas−solid fluidized beds. M.S. Thesis, University of British Columbia, British Columbia, Canada, 2000.

(8) Katz, H.; Sears, J. T. Electric field phenomena in fluidized and fixed beds. *Can. J. Chem. Eng.* **1969**, *47*, 50−53.

(9) Ali, F. S.; Ali, M. A.; Ali, R. A.; Inculet, I. I. Minority charge separation in falling particles with bipolar charge. *J. Electrost.* **1998**, *45*, 139−155.

(10) Boland, D.; Geldart, D. Electrostatic charging in gas fluidised beds. *Powder Technol.* **1971**, *5*, 289−297.

(11) Wolny, A.; Kazmierczak, W. Triboelectrification in fluidized bed of polystyrene. *Chem. Eng. Sci.* **1989**, *44* (11), 2607−2610.

(12) Ali, F. S.; Inculet, I. I.; Tedoldi, A. Charging of polymer powder inside a metallic fluidized bed. *J. Electrost.* **1999**, *45*, 199−211.

(13) Wolny, A.; Opalinski, I. Electric charge neutralization by addition of fines to a fluidized bed composed of coarse dielectric particles. *J. Electrost.* **1983**, *14*, 279−289.

(14) Tardos, G.; Pfeffer, R. A method to measure electrostatic charge on a granule in a fluidized bed. *Chem. Eng. Commun.* **1980**, *4*, 665−671.

(15) Fasso, L.; Chao, B. T.; Soo, S. L. Measurement of electrostatic charges and concentration of particles in the freeboard of a fluidized bed. *Powder Technol.* **1982**, *33*, 211−221.

(16) Chang, H.; Louge, M. Fluid dynamic similarity of circulating fluidized beds. *Powder Technol.* **1992**, *70*, 259−270.

(17) Jiang, P.; Bi, H.; Liang, S.-C.; Fan, L.-S. Hydrodynamic behavior of circulating fluidized bed with polymeric particles. *AIChE J.* **1994**, *40* (2), 193−206.

(18) Jiang, P.; Zhang, J.; Fan, L.-S. Electrostatic charge effects on the local solids distribution in the upper dilute region of circulating fluidized beds. In *Circulating Fluidized Beds V*; Kwauk, M., Li, J., Eds.; Science Press: Beijing 1997.

(19) Myler, C. A.; Zaltash, A.; Klinzing, G. E. Gas−solid transport in a 0.0508 m pipe at various inclinations with and without electrostatics II: Stability. *J. Powder Bulk Solids Technol.* **1986**, *10*, 13−17.

(20) Joseph, S.; Klinzing, G. E. Vertical gas−solid transition flow with electrostatics. *Powder Technol.* **1983**, *36*, 79−87.

(21) Zhang, Y.-F.; Yang, Y.; Arastoopour, H. Electrostatic effect on the flow behavior of a dilute gas/cohesive particle flow system. *AIChE J.* **1996**, *42* (6), 1590−1599.

(22) Plasynski, S. I.; Klinzing, G. E. High-pressure vertical pneumatic transport investigation. *Powder Technol.* **1994**, *79*, 95−109.

(23) Zaltash, A.; Myler, C.; Klinzing, G. E. Stability of gas−solid transport with electrostatics. *J. Pipelines* **1988**, *7*, 85−100.

(24) Liang, S.-C.; Zhang, J.-P.; Fan, L.-S. Electrostatic characteristics of hydrated lime powder during transport. *Ind. Eng. Chem. Res.* **1996**, *35*, 2748−2755.

(25) Dahn, C. J. Electrostatic hazards of pneumatic conveying of powders. *Saf. Consult. Eng.* **1992**, *11*, 201−204.

(26) Klinzing, G. E. Challenges in pneumatic conveying. *KONO* **2000**, *18*, 81−87.

(27) Lee, R. J.; Fan, L.-S. The effect of solid interaction forces on pneumatic handling of sorbent powders. *AIChE J.* **1993**, *39* (6), 1018−1029.

(28) Gupta, R.; Gidaspow, D.; Wasan, D. T. Electrostatic beneficiation of eastern oil shales. *Chem. Eng. Commun.* **1991**, *108*, 49−66.

(29) Plasynski, S. I.; Dhodapkar, S.; Klinzing, G. E. Observations from electrostatically charged conveying systems. Presented at NEPTIS-3, Kyoto, Japan, Nov 29−Dec 1, 1994.

(30) Dhodapkar, S. V. Flow pattern classification in gas−solid suspensions. Ph.D. Dissertation, University of Pittsburgh, Pittsburgh, PA, 1991; pp 62−76.

(31) Ebadat, V.; Singh, S. Importance of humidity on the control of electrostatic charging of high-density polyethylene powder. Presented at the Fourth International Conference on Pneumatic Conveying Technology, Glasgow, Scotland, Jun 26−28, 1990.

(32) Owen, P. R. Pneumatic transport. *J. Fluid Mech.* **1969**, *39* (2), 407−432.

(33) Klinzing, G. E.; Zaltash, A.; Myler, C. A. Particle velocity measurements through electrostatic field fluctuations using external probes. *Part. Sci. Technol.* **1987**, *5*, 95−104.

(34) Gajewski, A. Measuring the charging tendency of polystyrene particles in pneumatic conveyance. *J. Electrost.* **1989**, *23*, 55−66.

(35) Soo, S. L. Electrostatic hazards in pneumatic conveying. *J. Pipelines* **1981**, *1*, 57−68.

(36) Cole, B. N.; Baum, M. R.; Mobbs, F. R. An investigation of electrostatic charging effects in high-speed gas−solids pipe flows. *Proc. Inst. Mech. Eng.* **1969**, *184*, 77−83.

(37) Smeltzer, E. E.; Weaver, M. L.; Klinzing, G. E. Pressure drop losses due to electrostatic generation in pneumatic transport. *Ind. Eng. Chem. Process Des. Dev.* **1982**, *21*, 390−394.

(38) Ally, M. R.; Klinzing, G. E. Inter-relation of electrostatic charging and pressure drops in pneumatic transport. *Powder Technol.* **1985**, *44*, 85−88.

(39) Nieh, S.; Nguyen, T. Effects of humidity, conveying velocity, and particle size on electrostatic charges of glass beads in a gaseous suspension flow. *J. Electrost.* **1988**, *21*, 99−114.

(40) Soo, L. S.; Trezek, G. J. Turbulent pipe flow of magnesia. *Ind Eng. Chem. Fundam.* **1966**, *5*, 388−392.

(41) Neih, S.; Chao, B. T.; Soo, S. L. Modeling of pipe flow of a gas−solid suspension electrostatic and gravity effects. *J. Pipelines* **1987**, *7*, 73−84.

(42) Bailey, A. G. Electrostatic phenomena during powder handling. *Powder Technol.* **1984**, *37*, 71−85.

(43) Harper, W. R. *Contact and Frictional Electrification*; Oxford University Press: New York, 1967.

(44) Jones, T. B. *Electromechanics of Particles*; Cambridge University Press: New York, 1995.

(45) Sinclair, J. L.; Jackson, R. Gas−particle flow in a vertical pipe with particle−particle interaction. *AIChE J.* **1989**, *35*, 1473−1486.

(46) Bader, R.; Findlay, J.; Knowlton, T. M. Gas/solid flow patterns in a 30.5 cm diameter circulating fluidized bed. In *Circulating Fluidized Bed Technology II*; Basu, P., Large, J. F., Eds.; Permagon Press: New York, 1988; pp 123−137.

(47) Louge, M.; Mastorakos, E.; Jenkins, J. T. The role of particle collisions in pneumatic transport. *J. Fluid Mech.* **1991**, *231*, 345−359.

(48) Pita, J. A.; Sundaresan, S. Gas−solid flow in vertical tubes. *AIChE J.* **1991**, *37*, 1009−1018.

(49) Dasgupta, S.; Jackson, R.; Sundaresan, S. Turbulent gas−particle flow in vertical risers. *AIChE J.* **1994**, *40*, 215−228.

(50) Gidaspow, D. *Multiphase Flow and Fluidization*; Academic Press: New York, 1994.

(51) Hrenya, C. M.; Sinclair, J. L. Effects of particle-phase turbulence in gas−solid flows. *AIChE J.* **1997**, *43*, 853−869.

(52) Agrawal, K.; Loezos, P. N.; Syamlal, M.; Sundaresan, S. The role of meso-scale structures in rapid gas−solid flows. *J. Fluid Mech.* **2001**, *445*, 151−185.

(53) Grace, J. R.; Issangya, A. S.; Bai, D.; Bi, H. Situating the High-Density Circulating Fluidized Bed. *AIChE J.* **1999**, *45*, 2108−2116.

(54) Isangya, A. S.; Grace, J. R.; Bai, D.; Zhu, J. Further measurements of flow dynamics in a high-density circulating fluidized bed riser. *Powder Technol.* **2000**, *111*, 104−113.

(55) Pärssinen, J. H.; Zhu, J.-X. Axial and Radial Solids Distribution in a Long and High-Flux CFB Riser. *AIChE J.* **2001**, *47*, 2197−2205.

(56) Al-Adel. M. Role of Electrostatics on Gas−Particle Flows in Vertical Ducts. M.S. Thesis, Princeton University, Princeton, NJ, 2002, in preparation.

(57) Lun, C. K. K.; Savage, S. B.; Jeffrey, D. J.; Chepurniy, N. Kinetic theories of granular flows: Inelastic particles in Couette flow and slightly inelastic particles in a general flow field. *J. Fluid Mech.* **1984**, *140*, 223−256.

(58) Koch, D. L.; Sangani, A. S. Particle pressure and marginal stability limits for a homogeneous monodisperse gas fluidized bed: Kinetic theory and numerical simulations. *J. Fluid Mech.* **1999**, *400*, 229−263.

(59) Koch, D. L. Kinetic theory for a monodisperse gas−solid suspension. *Phys. Fluids A* **1990**, *2*, 1711−1723.

(60) Grace, J. R.; Avidan, A. A.; Knowlton, T. M. *Circulating Fluidized Beds*; Blackie Academic and Professional: New York, 1997.

(61) Bruggeman, D. A. G. *Ann. Phys.* **1935**, *24*, 636.

(62) Qi, C.; Farag, I. H. Lateral particle motion and its effect on particle concentration distribution in the riser of CFB. *AIChE Symp. Ser.* **1998**, *89* (296), 73−80.

Received for review December 5, 2001
Revised manuscript received January 22, 2002
Accepted January 23, 2002

IE010982W